Decay of ^{246}Bk* formed in similar entrance channel reactions of ^{11}B+^{235}U and ^{14}N+^{232}Th at low energies using the dynamical cluster-decay model

BirBikram Singh,[1] Manoj K. Sharma,[1] and Raj K. Gupta[2]
[1]*School of Physics and Material Science, Thapar University, Patiala-147004, India*
[2]*Department of Physics, Panjab University, Chandigarh-160014, India*
(Received 24 March 2008; published 28 May 2008)

The decay of the ^{246}Bk* nucleus, formed in entrance channel reactions ^{11}B+^{235}U and ^{14}N+^{232}Th at different incident energies, is studied by using the dynamical cluster-decay model (DCM) extended to include the deformations and orientations of nuclei. The main decay mode here is fission. The other (weaker) decay channels are the light particles evaporation ($A \leqslant 4$) and intermediate mass fragments ($5 \leqslant A \leqslant 20$). All decay products are calculated as emissions of preformed clusters through the interaction barriers. The calculated fission cross sections $\sigma_{\rm fiss}$, taken as a sum of the energetically favored symmetric and near symmetric fragments ($A_{\rm CN}/2 \pm 7$ and $A = 106$–110 plus complementary fragments) show an excellent agreement with experimental data at all experimental incident c.m. energies for both reactions, except for the top three energies in the case of the ^{11}B+^{235}U reaction. The disagreement between the DCM calculations and data at higher incident c.m. energies for the ^{11}B+^{235}U entrance channel is associated with the presence of additional effects of noncompound, quasifission (qf) components, in contradiction with the measured anisotropy effects which indicate the other entrance channel ^{14}N+^{232}Th to contain the noncompound nucleus contribution. The prediction of two fission windows, the symmetric fission (SF) and near symmetric or heavy mass fragments (HMFs), suggests the presence of a fine structure of fission fragments, which also need an experimental verification. The only parameter of the model is the neck length parameter $\triangle R$ whose value is shown to depend strongly on limiting angular momentum, which in turn depends on the use of sticking or nonsticking moment of inertia for angular momentum effects.

DOI: 10.1103/PhysRevC.77.054613 PACS number(s): 25.70.Jj, 23.70.+j, 24.10.−i

I. INTRODUCTION

A compound nucleus (CN) formed in low energy heavy ion reactions, in general, decays by emitting multiple light particles (n, p, α) and γ-rays resulting in the evaporation residue (ER) cross section, and is accompanied by a small (5–10%) component of so-called intermediate mass fragments (IMFs) of masses $5 \leqslant A \leqslant 20$ and charges $2 < Z < 10$ for both the light ($A_{\rm CN} \sim 40$–80) and medium mass ($A_{\rm CN} > 100$) compound systems. The production of IMFs in light compound nuclei is best understood in the extended Hauser-Feshbach (EHF) formalism of the BUSCO code [1] or the EHF method based on scission-point picture [2], and in medium mass nuclei as binary decay in the statistical fission model of Moretto [3]. For the lighter compound nuclei ($A_{\rm CN} < 80$), another fission model [4], called the saddle-point transition-state model, has also been successfully used. Apparently, in the above stated formalisms, the emission of light particles (LPs) is calculated within the Hauser-Feshbach method [5]. Alternatively, in the dynamical cluster-decay model [6–14], one of us (R.K.G.) and collaborators treated both the LPs and IMFs on an equal footing as the dynamical collective mass motions of preformed clusters through the barrier. The model is applied to both the light and medium mass systems, namely, the ^{48}Cr*, ^{56}Ni*, ^{116}Ba*, and ^{164}Yb* nuclei. In heavier CN ($A_{\rm CN} > 200$), like the ^{246}Bk* nucleus studied here, the main decay mode is (symmetric and near symmetric) fission which in DCM can be considered as an extreme case of IMFs, the heavier mass fragments (HMFs), observed together with or without the LPs and IMFs. In other words, all the processes of ER (LPs), IMFs as well as fission, or a combination of these, or any one of them alone as a dominant mode, can occur in different mass regions of the Periodic Table. In addition, there can be effects of noncompound nucleus decays, like pre-equilibrium fission, quasifission (qf), or deep inelastic collisions (DIC), etc., occurring mostly at higher incident center-of-mass (c.m.) energies.

The compound nucleus ^{246}Bk* formed in ^{11}B+^{235}U and ^{14}N+^{232}Th reaction channels at sub- and near-barrier energies [15,16] is highly fissile and decays almost totally by fission. Thus, fusion cross sections are nearly the same as the measured fission cross sections, which makes ^{246}Bk* an ideal case to study the compound nucleus fusion-fission process in heavy mass nuclei formed in low energy heavy ion reactions. Furthermore, the measured fission fragment anisotropies in these experiments [15,16] show the entrance channel effects for the anisotropy values of ^{11}B+^{235}U being consistent, but that of ^{14}N+^{232}Th anomalous, with respect to the statistical saddle-point model [4,17]. In other words, a noncompound nucleus component seems to be present in the fusion cross section for the ^{14}N+^{232}Th reaction. In this paper, we look for the dynamics of this effect with respect to different entrance channels of similar mass asymmetry on the basis of the dynamical cluster-decay model [6–14].

The dynamical cluster-decay model (DCM) for a hot and rotating nucleus, used here in this work, is described briefly in Sec. II. The effects of deformations and orientations of decay fragments are included. Application of the model to fusion-fission of ^{246}Bk* is discussed in Sec. III. This is a positive Q-value ($Q_{\rm out}$) system. Finally, Sec. IV gives a summary of our results. Interestingly, in contrast to the results of experiments

mentioned above, at higher incident c.m. energies we find the contributions of the quasifission process in the decay of ^{246}Bk* formed due to ^{11}B+^{235}U rather than due to the ^{14}N+^{232}Th incoming channel. In other words, the calculations on DCM show the decay of ^{246}Bk* formed via the ^{14}N+^{232}Th reaction as an almost pure CN decay.

II. THE DYNAMICAL CLUSTER-DECAY MODEL (DCM)

The dynamical cluster-decay model (DCM) is worked out in terms of the collective coordinates of mass and charge asymmetries $\eta = (A_1 - A_2)/(A_1 + A_2)$ and $\eta_Z = (Z_1 - Z_2)/(Z_1 + Z_2)$, the relative separation R, the multipole deformations $\beta_{\lambda i}$ ($\lambda = 2, 3, 4, \ldots$; $i = 1, 2$) and orientations θ_i of two nuclei or fragments. For the decay of the compound nucleus, the coordinates η and R refer, respectively, to nucleon division or exchange between outgoing fragments and the transfer of kinetic energy of the incoming channel ($E_{\rm c.m.}$) to internal excitation of the outgoing channel [the total kinetic energy TKE and total excitation energy TXE, related as $E^*_{\rm CN} + Q_{\rm out}(T) = {\rm TKE}(T) + {\rm TXE}(T)$, where the compound nucleus excitation energy $E^*_{\rm CN} = E_{\rm c.m.} + Q_{\rm in} = (A_{\rm CN}/9)T^2 - T$; T in MeV]. In terms of these coordinates, using partial waves, the compound nucleus decay cross section

$$\sigma = \sum_{\ell=0}^{\ell_{\max}} \sigma_\ell = \frac{\pi}{k^2} \sum_{\ell=0}^{\ell_{\max}} (2\ell + 1) P_0 P; \quad k = \sqrt{\frac{2\mu E_{\rm c.m.}}{\hbar^2}}, \tag{1}$$

where the preformation probability P_0 refers to η-motion and the penetrability P to R-motion, both depending on ℓ, T, $\beta_{\lambda i}$ and θ_i. The deformations of nuclei are kept to quadrupole deformations only ($\lambda = 2$), with their orientations as the optimal orientations of hot, i.e., compact configurations [18]. In Eq. (1), $\mu = [A_1 A_2/(A_1 + A_2)]m$ is the reduced mass with m as the nucleon mass. $\ell_{\max}$ is the maximum angular momentum, which could be used as a free parameter or else fixed for the vanishing of the fusion barrier of the incoming channel η_i or the light particle cross section $\sigma_{\rm LP} \to 0$. Equation (1) is used for the decay of the compound nucleus to LPs, complex IMFs, HMFs, and symmetric and/ or near symmetric fission (SF) fragments. The fission channel of ^{246}Bk* is taken to consist of both the HMFs and SF. For the competing, noncompound quasifission (qf) channel, the entrance channel is considered to keep its identity, and hence the preformation factor $P_0 = 1$ for qf.

The preformation probability $P_0[= \sqrt{B_{\eta\eta}} \mid \psi(\eta(A_i)) \mid^2 (2/A_{\rm CN})]$ is obtained by solving the stationary Schrödinger equation in η, at a fixed $R = R_a$,

$$\left\{ -\frac{\hbar^2}{2\sqrt{B_{\eta\eta}}} \frac{\partial}{\partial\eta} \frac{1}{\sqrt{B_{\eta\eta}}} \frac{\partial}{\partial\eta} + V_R(\eta, T) \right\} \psi_R^{(v)}(\eta) = E_R^{(v)} \psi_R^{(v)}(\eta), \tag{2}$$

where $R_a = R_1(\alpha_1,T) + R_2(\alpha_2,T) + \Delta R(\eta,T) = R_t(\alpha_i,T) + \Delta R(\eta, T)$, with the radius vectors

$$R_i(\alpha_i, T) = R_{0i}(T) \left[1 + \sum_\lambda \beta_{\lambda i} Y_\lambda^{(0)}(\alpha_i) \right]. \tag{3}$$

Here, $R_{0i}(T)$ are the temperature dependent nuclear radii for the equivalent spherical nuclei, given as [19]

$$R_{0i}(T) = \left[1.28 A_i^{1/3} - 0.76 + 0.8 A_i^{-1/3} \right] (1 + 0.0007 T^2). \tag{4}$$

In the above equations, α is the angle that the nuclear symmetry axis makes with a radius vector $R(\alpha)$, measured in the clockwise direction. This is to be distinguished from the orientation angle θ, in Eq. (5) below, that the nuclear symmetry axis makes with the collision Z-axis, measured in the anticlockwise direction (see Fig. 1 in [20]).

In Eq. (2), the mass parameters $B_{\eta\eta}$ are the smooth hydrodynamical masses [21], used for reasons of simplicity, and the fragmentation potential $V_R(\eta, T)$ is defined as

$$\begin{aligned} V_R(\eta, T) = &- \sum_{i=1}^{2} [V_{\rm LDM}(A_i, Z_i, T)] + \sum_{i=1}^{2} [\delta U_i] \exp\left(-\frac{T^2}{T_0^2} \right) \\ &+ V_P(R, A_i, \beta_{\lambda i}, \theta_i, T) + V_C(R, Z_i, \beta_{\lambda i}, \theta_i, T) \\ &+ V_\ell(R, A_i, \beta_{\lambda i}, \theta_i, T), \end{aligned} \tag{5}$$

where V_C, V_P, and V_ℓ are, respectively, the temperature and orientation dependent Coulomb, nuclear proximity, and angular momentum dependent potentials [18], respectively. The shell effects δU are obtained from the empirical estimates of Myers and Swiatecki [22], for spherical nuclei. Actually, the shell effects are also known to be strongly dependent on the deformation of the nucleus, but the nonavailability of a similar prescription for deformed nuclei limits our work to the approximation of spherical nuclei. The temperature dependent liquid drop energy $V_{\rm LDM}(T)$ in Eq. (5) is that of [23], which has the following form, based on the semi-empirical mass formula of Seeger [24]:

$$\begin{aligned} V_{\rm LDM}(A, Z, T) = &\alpha(T) A + \beta(T) A^{\frac{2}{3}} + \left(\gamma(T) - \frac{\eta(T)}{A^{\frac{1}{3}}} \right) \\ &\times \left(\frac{I^2 + 2|I|}{A} \right) + \frac{Z^2}{r_0(T) A^{\frac{1}{3}}} \\ &\times \left(1 - \frac{0.7636}{Z^{\frac{2}{3}}} - \frac{2.29}{[r_0(T) A^{\frac{1}{3}}]^2} \right) \\ &+ \delta(T) \frac{f(Z, A)}{A^{\frac{3}{4}}}, \end{aligned} \tag{6}$$

with

$$I = a_a(Z - N), \quad a_a = 1,$$

and, respectively, for even-even, even-odd, and odd-odd nuclei,

$$f(Z, A) = (-1, 0, 1).$$

Seeger [24] fitted the constants from ground-state ($T = 0$) binding energies of some 488 nuclei available at that time (in 1961) and obtained

$$\alpha(0) = -16.11 \text{ MeV}, \quad \beta(0) = 20.21 \text{ MeV},$$
$$\gamma(0) = 20.65 \text{ MeV}, \quad \eta(0) = 48.00 \text{ MeV},$$

and from Ref. [25], the pairing energy term

$$\delta(0) = 33.0 \text{ MeV}.$$

However, these constants are now readjusted in view of the availability of a large amount of data on ground-state binding

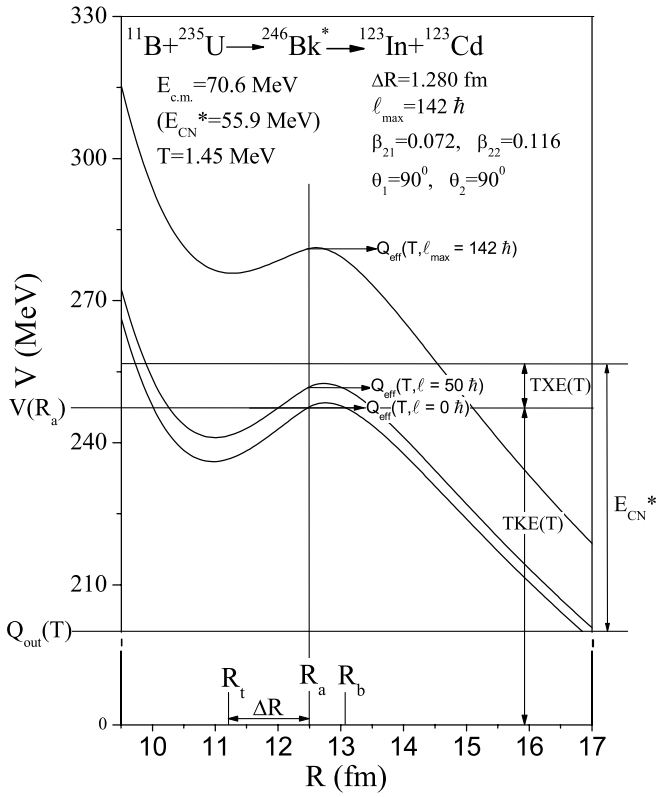

FIG. 1. Scattering potential for ^{246}Bk* → ^{123}In+^{123}Cd at temperature $T = 1.45$ MeV and different ℓ-values.

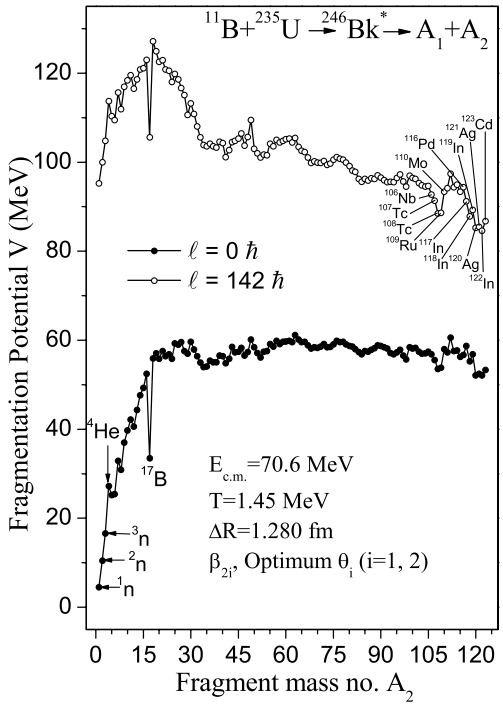

FIG. 2. The fragmentation potential as a function of the light fragment mass A_2 for the decay of ^{246}Bk*, formed in the ^{11}B+^{235}U reaction at $E_{c.m.} = 70.6$ MeV (equivalently, $T = 1.45$ MeV), calculated at two extreme ℓ-values.

energies [26]. A similar job was done in [8] for the 1995 Audi and Waspstra table of ground-state binding energies up to $Z = 56$, but we have redone it here for the new data [26] and now up to $Z = 97$, by defining the experimental binding energy $B_{\rm expt}$ of a nucleus as

$$B_{\rm expt} = V_{\rm LDM}(T = 0) + \delta U(T = 0).$$

Whenever the data were not available, the theoretical estimates of Moller *et al.* [27] were used. Since our aim here was simply to include the T-dependence on experimental binding energies, and not to obtain the new parameter set of $V_{\rm LDM}$, we have readjusted simply the bulk constant $\alpha(0)$ and the proton-neutron asymmetry constant a_a to obtain $B_{\rm expt}$ within <1.5 MeV. The temperature dependences of the constants of $V_{\rm LDM}$ in Eq. (6) are given in Fig. 1 of [23]. This procedure is particularly useful for light nuclei (including the neutron-proton-clusters, xn and xp, $x = 1, 2, 3\ldots$, defined in [28,29]) where shell corrections δU could not be defined on any shell model basis. Also, the missing deformation effects in spherical shell effects δU are included to some extent in the $V_{\rm LDM}$ since we essentially use the experimental binding energies split into two contributions ($V_{\rm LDM}$ and δU), and add the T-dependence to it.

The T-dependent, nuclear proximity potential for deformed, oriented nuclei [20],

$$V_P(s_0(T)) = 4\pi\,\bar{R}(T)\gamma b(T)\Phi(s_0(T)), \tag{7}$$

where $b(T) = 0.99(1 + 0.009T^2)$ is the nuclear surface thickness, $\gamma = 0.9517[1 - 1.7826(\frac{N-Z}{A})^2]$ MeV fm^{-2}, the surface energy constant and $\bar{R}(T)$ is the mean curvature radius (for details see Ref. [20]). Φ in Eq. (7) is the universal function, independent of the shapes of nuclei or the geometry of nuclear system, but depends on the minimum separation distance $s_0(T)$ (see Fig. 2 in [20]), as

$$\Phi(s_0) = \begin{cases} -\frac{1}{2}(s_0(T) - 2.54)^2 - 0.0852(s_0(T) - 2.54)^3 \\ -3.437\exp\left(-\frac{s_0(T)}{0.75}\right), \end{cases} \tag{8}$$

respectively, for $s_0(T) \leqslant 1.2511$ and $s_0(T) \geqslant 1.2511$. The Coulomb potential for a multipole-multipole interaction between two separated nuclei

$$V_C = \frac{Z_1 Z_2 e^2}{R} + 3Z_1 Z_2 e^2 \sum_{\lambda,i=1,2} \times \frac{R_i^\lambda(\alpha_i, T)}{(2\lambda+1)R^{\lambda+1}} Y_\lambda^{(0)}(\theta_i)\left[\beta_{\lambda i} + \frac{4}{7}\beta_{\lambda i}^2 Y_\lambda^{(0)}(\theta_i)\right], \tag{9}$$

and the angular momentum dependent potential,

$$V_\ell = \frac{\hbar^2\ell(\ell+1)}{2I_s} \tag{10}$$

with moment-of-inertia in the sticking limit

$$I_S = \mu R^2 + \tfrac{2}{5}A_1 m R_1^2(\alpha_1, T) + \tfrac{2}{5}A_2 m R_2^2(\alpha_2, T). \tag{11}$$

Note that, in general, the experimental numbers for angular momentum ℓ are based on the moment of inertia calculated [30] in the nonsticking limit ($I_{\rm NS} = \mu R^2$). However, this use of the reduced mass alone corresponds to the supposition that the emission of the fragment is punctual, and there are also

other possible hypotheses aside from the sticking limit such as the rolling or sliding conditions. We find that the sticking limit (I_S) used here is more appropriate for the proximity potential (nuclear surfaces $\leqslant$2 fm apart) which has the consequence that the limiting ℓ-value is much larger in this case. In the following, we shall see that the use of a larger $\ell_{\max}$-value due to a relatively larger magnitude of I_S results in a reduction of the nuclear surface separation distance ΔR for nuclear collisions [31], and vice versa for $I_{\rm NS}$.

Normalizing $V_R(\eta, T)$ to the channel binding energy, we get the scattering potential $V(R, T)$, illustrated in Fig. 1 for the exit channel ^{123}In+^{123}Cd. For such a potential, the tunneling probability P is the WKB integral,

$$P = \exp\left(-\frac{2}{\hbar}\int_{R_a}^{R_b}\{2\mu[V(R) - Q_{\rm eff}]\}^{1/2}dR\right) \qquad (12)$$

with

$$V(R_a) = V(R_b) = Q_{\rm eff} = {\rm TKE}(T).$$

Here, the potential $V(R_a)$ corresponds to the first turning point $R = R_a = R_t(\eta, T) + \Delta R(T)$, which can be looked upon as an effective, positive Q-value, $Q_{\rm eff}$, for the decay of the hot compound nucleus, like the $Q_{\rm out}$-value in spontaneous cluster decay [for $T = 0$, $R_a = R_t(\eta)$ and ${\rm TKE}(T = 0) = Q_{\rm out}$]. R_b is the second turning point. Since we do not know how to add the ℓ effects in the binding energies, the ℓ-dependence of R_a is defined by

$$V(R_a, \ell) = Q_{\rm eff}(T, \ell = 0),$$

i.e., R_a is taken to be the same for all ℓ-values, and that $Q_{\rm eff}(T, \ell) = V(R_a, \ell)$. Note, ΔR is in fact η-dependent, but here in the following we have used an average T-dependent value. For further details, see [11].

III. CALCULATIONS AND DISCUSSIONS

As already mentioned above, fission cross sections for the decay of ^{246}Bk*, formed in ^{11}B+^{235}U and ^{14}N+^{232}Th reactions, have been measured [16] at various $E_{\rm c.m.}$, which represent the sole contribution to the total fusion cross section ($\sigma_{\rm fus}^{\rm Expt} = \sigma_{\rm fiss}^{\rm Expt}$). No contribution due to the emission of LPs ($A \leqslant 4$), IMFs ($4 \leqslant A \leqslant 20$) or noncompound qf processes are explicitly recorded.

Figure 2 shows the calculated fragmentation potentials for the decay of ^{246}Bk* (formed in the ^{11}B+^{235}U reaction at $E_{\rm c.m.} = 70.6$ MeV or $T = 1.45$ MeV) at two extreme $\ell = 0$ and $\ell_{\max}$-values, using quadrupole deformations and optimally oriented hot configurations according to Table 1 of Ref. [18]. $\ell_{\max} = 142\hbar$ is fixed for $\sigma_{\rm LPs} \to 0$ (see Fig. 5 below). We note that the LPs and IMFs are favored (lower in energy) at $\ell = 0$, but at higher ℓ-values the symmetric and near-symmetric fragments become more favored. At $\ell = 142\hbar$, a strong minima is obtained for symmetric fragments $A = 116$–123, denoted as the symmetric fission (SF) window of mass $A_{\rm CN}/2 \pm 7$. Also, another minima is seen in the immediate neighborhood of the SF window, corresponding to heavy mass fragments $A = 106$–110, referred to as the HMFs window. Thus, a sum of the SF and HMFs windows in Fig. 2 gives

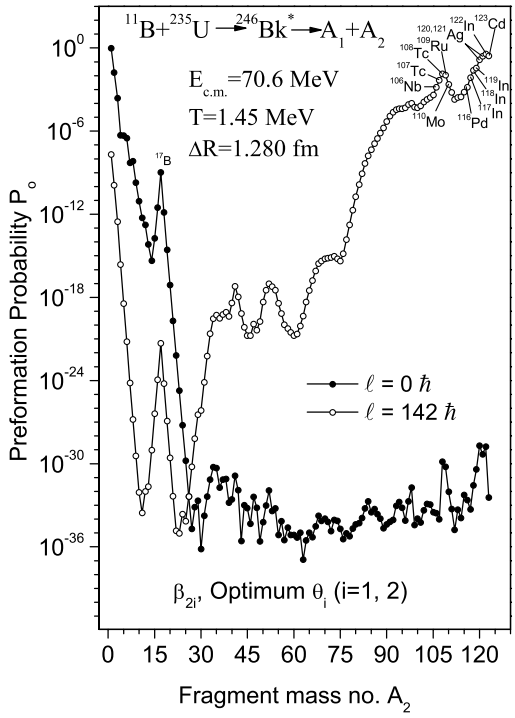

FIG. 3. Same as for Fig. 2, but for the preformation probability P_0.

the (total) fission of the compound nucleus. Since the reported fission cross sections correspond to assumed symmetric mass division only [16], without actually identifying the fragments, the presence of a new HMFs window, in addition to the SF window, allows us to look for the fine- or substructure of the fission of ^{246}Bk* (see below, Fig. 8).

The above result of a favored asymmetric to a favored symmetric division with increase in ℓ-value is also depicted in Fig. 3 for the preformation factor $P_0(A_2)$, and in Fig. 4 for the penetration probability $P(A_2)$. In Fig. 4, we notice that, at higher ℓ-value, $P \to 1$ (its highest value) for the symmetric fragments. P is very small for the emission of LPs, and also tends to zero for the ^{17}B fragment (so also for ^{18}B) which occurs as a strong minimum in the fragmentation potential of Fig. 2 or as a maximum in the preformation probability of Fig. 3. In the following, we shall see that a major contribution to the fission (equivalently, fusion) cross section arises from the SF window, and that the HMFs window contributes to a maximum of ~5% and that too only for the first few higher c.m. (top three) energies. Furthermore, we shall see that the entrance channel also plays its role in terms of the quasifission contributing, at higher c.m. energies, due to the ^{11}B+^{235}U reaction and *not* due to the ^{14}N+^{232}Th reaction. Thus, in our calculations, respectively, for the case of negligible or zero contributions from LPs and IMFs, $\sigma_{\rm fus}^{\rm Cal} = \sigma_{\rm HMFs} + \sigma_{\rm SF} + \sigma_{\rm qf} = \sigma_{\rm fiss}^{\rm Cal} + \sigma_{\rm qf}$, to be compared with experimentally measured $\sigma_{\rm fus}^{\rm Expt} (= \sigma_{\rm fiss}^{\rm Expt})$. Apparently, the quasifission component is obtained empirically [32] as the difference between the experimentally measured and our calculated fission components, i.e., $\sigma_{\rm qf} = \sigma_{\rm fiss}^{\rm Expt} - \sigma_{\rm fiss}^{\rm Cal}$.

Figure 5 presents the calculated cross section as a function of angular momentum for the LPs ($A = 1$–4 summed)

TABLE I. The decay cross sections for LPs, $\sigma_{\rm LPs}$, the symmetric fission (SF) window ($A = A_{\rm CN}/2 \pm 7$), $\sigma_{\rm SF}$, the heavy mass fragments (HMFs) window (A = 106–110, and their complementary fragments), $\sigma_{\rm HMFs}$, and the quasifission (qf) component, $\sigma_{\rm qf}$, and their sums $\sigma_{\rm fiss}^{\rm Cal}(=\sigma_{\rm SF}+\sigma_{\rm HMFs})$ and $\sigma_{\rm fus}^{\rm Cal}(=\sigma_{\rm qf}+\sigma_{\rm fiss}^{\rm Cal})$, calculated on DCM for different $E_{\rm c.m.}$ for ^{246}Bk* formed in the ^{11}B+^{235}U reaction, compared with the experimental fusion (≡ fission) cross sections [16], $\sigma_{\rm fus}^{\rm Expt}(\equiv\sigma_{\rm fiss}^{\rm Expt})$.

				DCM					DCM ($P_0 = 1$)		Cal	Expt
$E_{\rm c.m.}$ (MeV)	$E^*_{\rm CN}$ (MeV)	T (MeV)	$\ell_{\rm max}$ ($\hbar$)	ΔR (fm)	$\sigma_{\rm LP}$ (mb)	$\sigma_{\rm fiss}^{\rm Cal}$(mb) $\sigma_{\rm SF}$	$\sigma_{\rm HMFs}$	Sum	ΔR (fm)	$\sigma_{\rm qf}$ (mb)	$\sigma_{\rm fus}^{\rm Cal}(=\sigma_{\rm fiss}^{\rm Cal}+\sigma_{\rm qf})$ (mb)	$\sigma_{\rm fus}^{\rm Expt}(\equiv\sigma_{\rm fiss}^{\rm Expt})$ (mb)
70.6	55.9	1.449	142	1.2800	9.06×10^{-2}	1080.11	50.46	1130.57	1.167	310.93	1441.50	1440 ± 138
68.7	54.0	1.424	142	1.2800	9.29×10^{-2}	1125.76	51.80	1177.56	1.133	214.44	1392.00	1390 ± 128
66.8	52.0	1.398	141	1.2800	9.03×10^{-2}	1115.45	46.23	1161.68	1.000	44.33	1206.01	1200 ± 112
64.9	50.1	1.372	140	1.1760	1.11×10^{-2}	1017.71	14.54	1032.25	0.943	20.35	1052.60	1030 ± 72
63.0	48.2	1.346	140	1.1470	5.62×10^{-3}	954.51	10.62	965.13	0.887	9.64	974.77	960 ± 95
61.0	46.3	1.320	140	1.1300	3.82×10^{-3}	761.18	8.41	769.59	0.828	4.08	773.67	772 ± 54
59.1	44.4	1.293	140	1.1171	2.91×10^{-3}	621.96	7.31	629.27	0.775	1.81	631.08	630 ± 40.0
57.2	42.5	1.266	140	1.0940	1.75×10^{-3}	461.40	5.32	466.73	0.724	0.85	467.58	465 ± 33
55.3	40.6	1.237	139	1.0540	5.41×10^{-4}	269.36	2.70	272.06	0.672	0.36	272.42	270 ± 20.0
53.4	38.7	1.208	139	1.0130	6.94×10^{-5}	130.88	1.06	131.94	0.620	0.17	132.11	132 ± 14.0
51.5	36.8	1.179	137	0.9940	1.70×10^{-5}	54.78	0.35	55.13	0.572	0.07	55.20	54.6 ± 5.3
49.0	34.3	1.139	137	0.9470	3.51×10^{-7}	7.20	0.03	7.23	0.507	0.03	7.26	7.00 ± 2.0

compared with the same for the symmetric fragment $A = A_{\rm CN}/2 = 123$ alone, up to $\ell_{\rm max} = 142\hbar$ where the $\sigma_{\rm LPs}(\ell)$ goes to zero. We note that the contribution of light-particles cross section $\sigma_{\rm LPs}$, summed up to $\ell_{\rm max}$ (given in the braces of the legend), is almost zero compared to the cross section of symmetric fragment alone.

Figure 6 gives a comparison of our DCM calculated fission cross sections $\sigma_{\rm fiss}^{\rm Cal}(=\sigma_{\rm SF}+\sigma_{\rm HMFs}$, hollow squares) at different center-of-mass energies, with the experimental data [16] on $\sigma_{\rm fiss}^{\rm Expt}(\equiv\sigma_{\rm fus}^{\rm Expt}$, filled circles) for the ^{11}B+^{235}U reaction channel. The same result is also presented in Table I along with other calculated quantities and fitted parameters. Within one parameter fit, the comparison is clearly very good, except at the highest three energies. This discrepancy is associated with the presence of a significant noncompound, quasifission contribution at these three energies. This is explicitly calculated on DCM ($P_0 = 1$) for the best fit to the empirically estimated $\sigma_{\rm qf}(=\sigma_{\rm fiss}^{\rm Expt}-\sigma_{\rm fiss}^{\rm Cal})$, also shown in

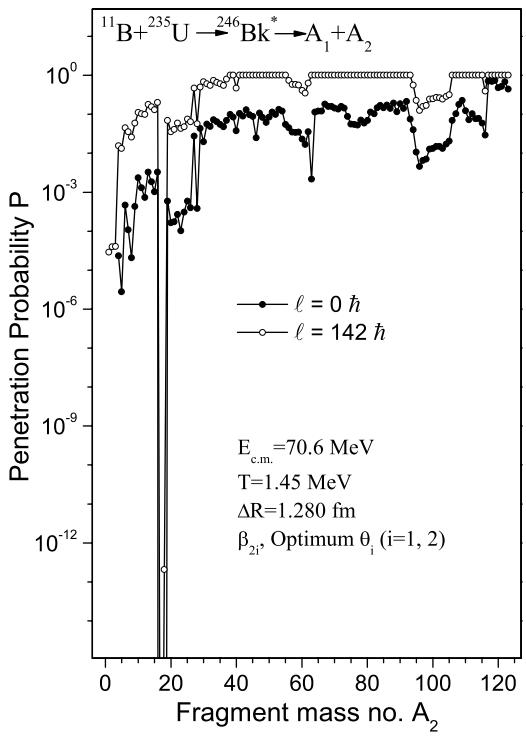

FIG. 4. Same as for Fig. 2, but for the penetration probability P.

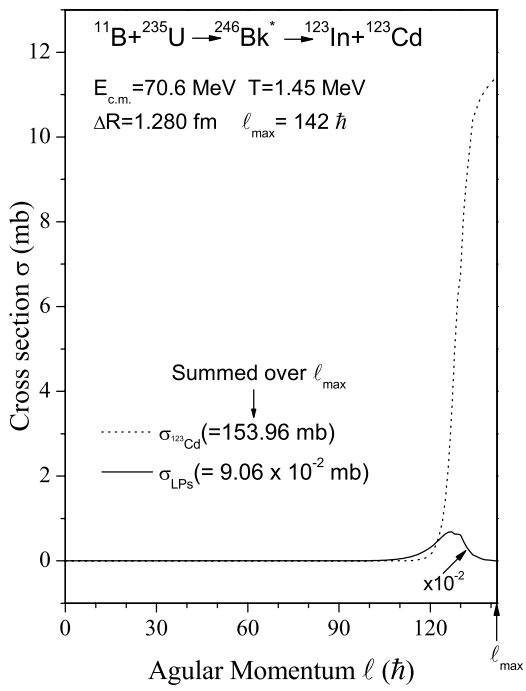

FIG. 5. Variation of $\sigma_{A=123}$, the cross section for symmetric fission fragment of mass $A = 123$, and the summed up cross section for LPs (A = 1–4), the $\sigma_{\rm LPs}$, as a function of the angular momentum ℓ for the decay of ^{246}Bk* (formed in ^{11}B+^{235}U reaction at T = 1.45 MeV) up to a point where $\sigma_{\rm LPs} \to 0$.

TABLE II. Same as for Table I, but for the reaction ^{14}N+^{232}Th, and without the quasifission (qf) component.

				DCM					Expt
$E_{c.m.}$ (MeV)	E^*_{CN} (MeV)	T (MeV)	ℓ_{max} ($\hbar$)	$\triangle R$ (fm)	σ_{LP} (mb)	σ^{Cal}_{fiss}(mb) σ_{SF}	σ_{HMFs}	Sum	$\sigma^{Expt}_{fiss}(\equiv \sigma^{Expt}_{fus})$ (mb)
86.4	60.9	1.511	142	1.2360	3.45×10^{-2}	782.04	41.24	823.29	823 ± 40
82.5	57.0	1.463	142	1.1410	5.05×10^{-3}	641.49	10.73	652.21	650 ± 26
79.9	54.4	1.429	142	1.1255	3.65×10^{-3}	510.35	9.79	520.14	518 ± 24
78.0	52.5	1.404	141	1.1110	2.58×10^{-3}	369.47	7.48	376.95	380 ± 53
76.1	50.6	1.379	141	1.0860	1.41×10^{-3}	285.02	5.45	290.48	290 ± 27
74.2	48.7	1.353	140	1.0640	7.57×10^{-4}	211.12	3.46	214.58	214 ± 11
72.2	46.8	1.327	140	1.0200	1.51×10^{-4}	108.27	1.47	109.74	111 ± 07
70.4	44.9	1.300	140	0.9950	3.20×10^{-5}	54.35	0.64	55.00	54 ± 04
68.5	43.0	1.273	139	0.9700	5.77×10^{-6}	19.69	0.17	19.85	20.3 ± 2

Fig. 6 as open down-triangles. The sum of our calculated fission component σ^{Cal}_{fiss} and quasifission σ_{qf} is plotted here as σ^{Cal}_{fus} (open up-triangles) which shows an excellent comparison with experimental fusion cross sections $\sigma^{Expt}_{fus}(\equiv \sigma^{Expt}_{fiss})$. Apparently, the quasifission cross section contributes only for the top three energies, and is negligibly small at all lower energies. We have also listed in Table I, and plotted in Fig. 6, our calculated σ_{LPs} contribution which is also negligibly small at all energies, and decreases with decreasing c.m. energies in agreement with an earlier study [33].

For the incident channel ^{14}N+^{232}Th, our results on DCM are presented in Fig. 7 and Table II, compared with the experimental data of Ref. [16]. The important result is that ^{14}N+^{232}Th is a pure CN reaction, showing no quasifission contribution, in disagreement with the anisotropy results of Behera *et al.* [16]. Hence, a further experimental check of this result is called for. For the calculated fission cross section, however, the two contributing windows (SF and HMFs) show nearly the same fine- or substructure effect, depicted in Fig. 8 for both incoming channels. Here, peak 2 corresponds to fragment mass $A = 108$ for the first three highest energies of channel ^{11}B+^{235}U and for only the first highest energy of channel ^{14}N+^{232}Th, and to fragment mass $A = 109$ for the rest of the energies in both channels since the peak shifts between $A = 108$ and $A = 109$. Peak 1 corresponds to fragment mass $A = 122$. The peaks for the two windows are marked, for example, in Fig. 3. An experimental verification of such a substructure of fission yields would also be interesting.

Finally, we look at the only free parameter of the model, the length parameter $\triangle R$ and its connection to the ℓ_{max}-value due to the use of the sticking or nonsticking moment of inertia. All

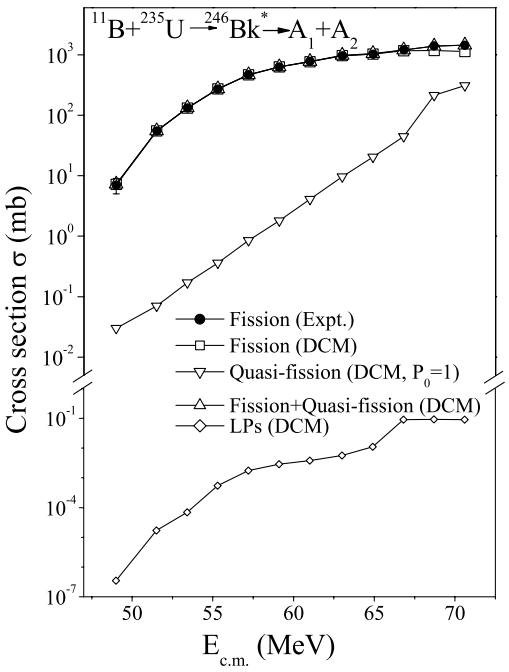

FIG. 6. The calculated σ^{Cal}_{fus}, $\sigma^{Cal}_{fiss}(= \sigma_{SF} + \sigma_{HMFs})$, empirical σ_{qf} and σ_{LPs} on DCM for the decay of compound nucleus ^{246}Bk* formed in the ^{11}B+^{235}U reaction at various $E_{c.m.}$, compared with experimental data [16] on $\sigma^{Expt}_{fus}(\equiv \sigma^{Expt}_{fiss})$.

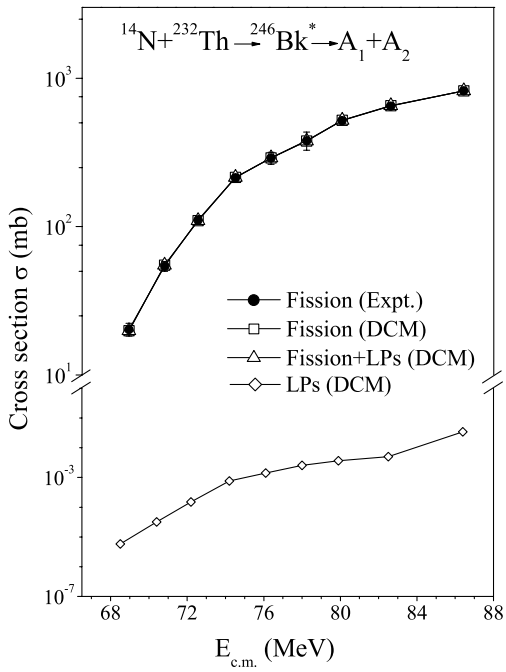

FIG. 7. Same as for Fig. 6, but for the ^{14}N+^{232}Th reaction.

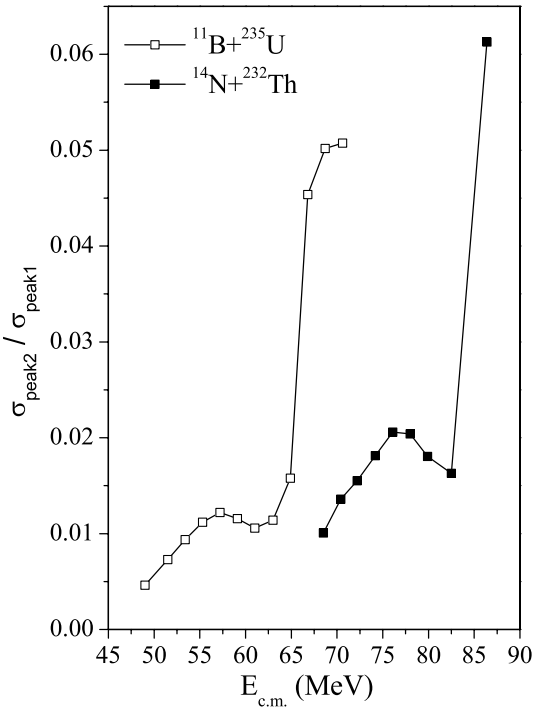

FIG. 8. The ratios of the peak values of HMFs window and SF window as a function of the incident $E_{\mathrm{c.m.}}$.

the calculations presented above are for the sticking moment of inertia I_S where $\ell_{\max}$ is fixed for $\sigma_{\mathrm{LPs}} \to 0$, and is found to decrease slowly with decreasing $E_{\mathrm{c.m.}}$ (see Tables I, II, and Fig. 9). Figure 9 gives the variation of $\triangle R$ with $E_{\mathrm{c.m.}}$ for fission (dotted line with solid squares) and quasifission (dotted line with hollow circles) in the case of entrance channel ^{11}B+^{235}U, and for fission alone for the entrance channel ^{14}N+^{232}Th since the quasifission component is zero in this later case. We observe that $\triangle R$ increases with increasing $E_{\mathrm{c.m.}}$ for both processes, showing a similar behavior in the case of fission for the two entrance channels (the two straight line fits have nearly the same slope). The interesting result is that fission occurs earlier ($\triangle R$ larger) than quasifission, and that qf is simply an additional contribution to fusion cross section rather than a competing process of the type observed in, for example, ^{48}Ca induced reactions on deformed actinides for the synthesis of superheavy nuclei [34].

Next, as an illustrative case, we use for quasifission the nonsticking moment of inertia I_{NS} and find that for a similar fit as above for I_S, $\ell_{\max}$ decreases considerably ($\ell_{\max} = 31$ and $23\hbar$, respectively, for $E_{\mathrm{c.m.}} = 70.6$ and 49.0 MeV, instead of 142 and $137\hbar$) but then $\triangle R$ increases significantly [see solid line with crosses in Fig. 9(a)], approaching almost the value for fission for use of I_S [the dashed line with solid squares in Fig. 9(a)]. The interesting result is that for qf, nearly the same $\triangle R(E_{\mathrm{c.m.}})$ variation is obtained for I_S at $\ell_{\max} = 66\hbar$ [solid line with open circles in Fig. 9(a)] as is obtained above (solid line with crosses) for I_{NS} at about half the $\ell_{\max}$-value. The $\ell_{\max} = 66\hbar$ matches exactly the value given by the finite-range liquid drop model (FRLDM) for mass $A = 246$ compound nucleus (see Fig. 1 in [35]). For heavy ion collisions, however, we consider the sticking moment of inertia as more appropriate,

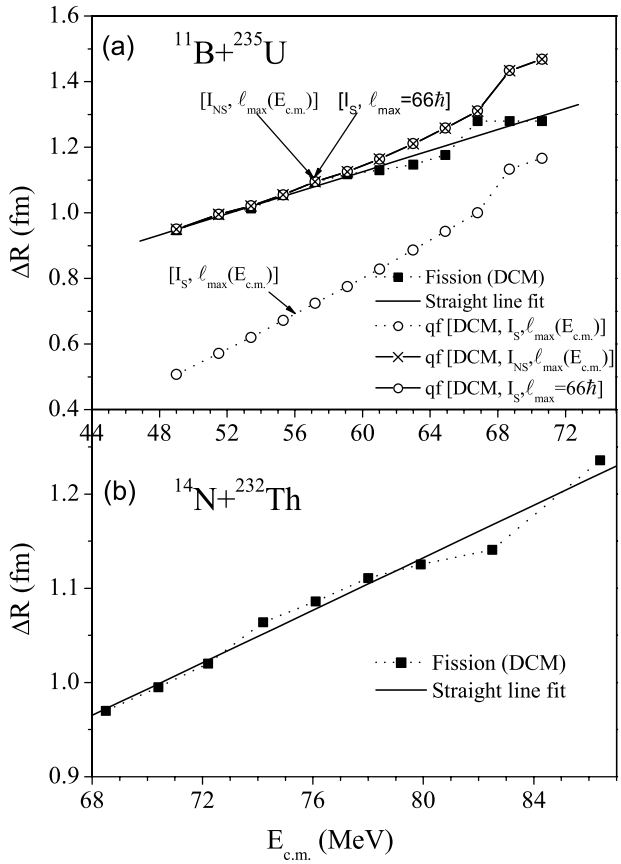

FIG. 9. (a) The fitted parameter $\triangle R$ for fission (dotted line with solid squares) and quasifission (dotted line with hollow circles) decays of the CN formed in the ^{11}B+^{235}U reaction as a function of $E_{\mathrm{c.m.}}$. (b) The same for fission decay in the case of the reaction ^{14}N+^{232}Th. Straight line fits $\triangle R = 0.162 + 0.016E_{\mathrm{c.m.}}$ and $\triangle R = 0.018 + 0.014E_{\mathrm{c.m.}}$, respectively, for ^{11}B+^{235}U and ^{14}N+^{232}Th are also shown as solid lines.

which involves a larger limiting value for ℓ and hence a smaller neck length parameter $\triangle R$. Also, the data on TKE favors the use of I_S, as compared to I_{NS} (see Fig. 7 in [7]).

IV. SUMMARY

In this paper, we have studied the decay of ^{246}Bk* formed in reaction channels ^{11}B+^{235}U and ^{14}N+^{232}Th at different center-of-mass energies. The results of the DCM calculations, using hot (compact) configurations for quadrupole deformed nuclei, are compared with the experimental data [16]. Our calculations clearly demonstrate that, independent of the entrance channel, the decay of ^{246}Bk* into symmetric and near-symmetric fragments are highly favored over the light particles (LPs) and intermediate mass fragments (IMFs), in particular at higher angular momentum ℓ-values. At $\ell = \ell_{\max}$, the preformation factor P_0 is large and penetration probability P approaches unity for all the symmetric and near-symmetric fragments. Thus, the main contribution to the decay cross section comes from the fusion-fission fragments which consist of the symmetric fission (SF) window of mass $A_{\mathrm{CN}}/2 \pm 7$ and a

heavy mass fragments (HMFs) window of $A = 106$–110 (and complementary fragments) in the immediate neighborhood of the SF window. Interestingly, the prediction of two windows suggests a fine- or substructure of observed fission fragments, not yet analyzed experimentally.

For the entrance channel $^{11}B+^{235}U$, the DCM calculations are in good agreement with the experimental data for all c.m. energies, except for the highest three energies. Allowing a contribution from the noncompound quasifission (qf) process makes the comparison very good at all experimental energies. The cross section for qf, σ_{qf}, is significant for only the top three energies. For the $^{14}N+^{232}Th$ entrance channel, however, contrary to the experimental observations (of anisotropy), the noncompound nucleus (quasifission) contribution is zero, i.e., the DCM calculated $\sigma_{fiss}^{Cal}(= \sigma_{SF} + \sigma_{HMFs})$ matches the measured fission cross section $\sigma_{fiss}^{Expt}(\equiv \sigma_{fus}^{Expt})$ almost exactly without invoking any quasifission contribution. Note, however, that there is a parameter (the length parameter $\triangle R$) to be fitted in this model, which shows a simple linear dependence on the incident c.m. energy, with an almost constant slope for both the entrance channels. The role of sticking versus nonsticking moment of inertia for the limiting angular momentum ℓ_{max} is also studied, which results in an increase of $\triangle R$ for the lower ℓ_{max}-value of I_{NS} used in experiments.

ACKNOWLEDGMENTS

The authors are thankful to Dr. S. Kailas, BARC, Mumbai (India) for a useful discussion. One of us (M.K.S.) is thankful to University Grants Commision, New Delhi for financial support for this work in form of a research project, and another of us (R.K.G.) to Department of Science and Technology, Govt. of India, for support in terms of a Ramanna research grant.

[1] J. Gomez del Campo, R. L. Auble, J. R. Beene, M. L. Halbert, H. J. Kim, A. D'Onofrio, and J. L. Charvet, Phys. Rev. C **43**, 2689 (1991).
[2] T. Matsuse, C. Beck, R. Nouicer, and D. Mahboub, Phys. Rev. C **55**, 1380 (1997).
[3] L. G. Moretto, Nucl. Phys. **A247**, 211 (1975).
[4] R. Vandenbosch and J. R. Huizenga, *Nuclear Fission* (Academic, New York, 1973).
[5] S. J. Sanders, A. Szanto de Toledo, and C. Beck, Phys. Rep. **311**, 487 (1999).
[6] R. K. Gupta, M. Balasubramaniam, C. Mazzocchi, M. LaCommara, and W. Scheid, Phys. Rev. C **65**, 024601 (2002).
[7] R. K. Gupta, R. Kumar, N. K. Dhiman, M. Balasubramaniam, W. Scheid, and C. Beck, Phys. Rev. C **68**, 014610 (2003).
[8] M. Balasubramaniam, R. Kumar, R. K. Gupta, C. Beck, and W. Scheid, J. Phys. G: Nucl. Part. Phys. **29**, 2703 (2003).
[9] R. K. Gupta, Acta Phys. Hung. New Ser. Heavy Ion Phys. **18**, 347 (2003).
[10] R. K. Gupta, M. Balasubramaniam, R. Kumar, D. Singh, and C. Beck, Nucl. Phys. **A738**, 479c (2004).
[11] R. K. Gupta, M. Balasubramaniam, R. Kumar, D. Singh, C. Beck, and W. Greiner, Phys. Rev. C **71**, 014601 (2005).
[12] R. K. Gupta, M. Balasubramaniam, R. Kumar, D. Singh, S. K. Arun, and W. Greiner, J. Phys. G: Nucl. Part. Phys. **32**, 345 (2006).
[13] B. B. Singh, M. K. Sharma, R. K. Gupta, and W. Greiner, Int. J. Mod. Phys. E **15**, 699 (2006).
[14] S. K. Arun and R. K. Gupta, Chandigarh preprint, to be published.
[15] B. R. Behera, S. Jena, M. Satpathy, S. Kailas, K. Mahata, A. Shrivastava, A. Chatterjee, S. Roy, P. Basu, M. K. Sharan, and S. K. Datta, Phys. Rev. C **64**, 041602(R) (2001).
[16] B. R. Behera, M. Satpathy, S. Jena, S. Kailas, R. G. Thomas, K. Mahata, A. Chatterjee, S. Roy, P. Basu, M. K. Sharan, and S. K. Datta, Phys. Rev. C **69**, 064603 (2004).
[17] S. Kailas, Phys. Rep. **284**, 381 (1997).
[18] R. K. Gupta, M. Balasubramaniam, R. Kumar, N. Singh, M. Mahhas, and W. Greiner, J. Phys. G: Nucl. Part. Phys. **31**, 631 (2005).
[19] G. Royer and J. Mignen, J. Phys. G: Nucl. Part. Phys. **18**, 1781 (1992).
[20] R. K. Gupta, N. Singh, and M. Manhas, Phys. Rev. C **70**, 034608 (2004).
[21] H. Kröger and W. Scheid, J. Phys. G: Nucl. Phys. **6**, L85 (1980).
[22] W. D. Myers and W. J. Swiatecki, Nucl. Phys. **81**, 1 (1966).
[23] N. J. Davidson, S. S. Hsiao, J. Markram, H. G. Miller, and Y. Tzeng, Nucl. Phys. **A570**, 61c (1994).
[24] P. A. Seeger, Nucl. Phys. **25**, 1 (1961).
[25] S. DeBenedetti, *Nuclear Interactions* (Wiley, New York, 1964).
[26] G. Audi, A. H. Wapstra, and C. Thiboult, Nucl. Phys. **A729**, 337 (2003).
[27] P. Moller, J. R. Nix, W. D. Myers, and W. J. Swiatecki, At. Data Nucl. Data Tables **59**, 185 (1995).
[28] R. K. Gupta, S. Kumar, M. Balasubramaniam, G. Münzenberg, and W. Scheid, J. Phys. G: Nucl. Part. Phys. **28**, 699 (2002).
[29] R. K. Gupta, M. Balasubramaniam, S. Kumar, S. K. Patra, G. Münzenberg, and W. Greiner, J. Phys. G: Nucl. Part. Phys. **32**, 565 (2006).
[30] S. Kailas (private communication).
[31] R. Kumar, D. Singh, N. Sharma, and R. K. Gupta, Contribution to the 2nd Chandigarh Science Congress, Chandigarh, March 14–15, 2008.
[32] G. N. Knyazheva, E. M. Kozulin, R. N. Sagaidak, A. Yu. Chizhov, M. G. Itkis, N. A. Kondratiev, V. M. Voskressensky, A. M. Stefanini, B. R. Behera, L. Corradi, E. Fioretto, A. Gadea, A. Latina, S. Szilner, M. Trotta, S. Beghini, G. Montagnoli, F. Scarlassara, F. Haas, N. Rowley, P. R. S. Gomes, and A. Szanto de Toledo, Phys. Rev. C **75**, 064602 (2007).
[33] H. Delagrange, C. Gregoire, F. Scheuter, and Y. Abe, Z. Phys. A - Atomic Nuclei **323**, 437 (1986).
[34] M. G. Itkis, A. A. Bogatchev, I. M. Itkis, M. Jandel, J. Kliman, G. N. Kniajeva, N. A. Kondratiev, I. V. Korzyukov, E. M. Kozulin, L. Krupa, Yu. Ts. Oganessian, I. V. Pokrovski, V. A. Ponomarenko, E. V. Prokhorova, A. Ya. Rusanov, V. M. Voskresenski, A. A. Goverdovski, F. Hanappe, T. Materna, N. Rowley, L. Stuttge, G. Giardina, and K. J. Moody, J. Nucl. Radiochem. Sci. **3**, 57 (2002).
[35] C. Beck and A. Szanto de Toledo, Phys. Rev. C **53**, 1989 (1996).